Desalination and Water Treatment
www.deswater.com

doi: 10.5004/dwt.2023.29282

284 (2023) 87–100
February

Optimization of adsorption parameters for pesticides removal using bentonite-layered double hydroxide by response surface methodology

Dania K. Ali[a,*], Ahmed A. Mohammed[b]

[a]*Department of Diwan Affairs, Presidency of the University of Baghdad, Baghdad, Iraq, email: eng.dania277@gmail.com*
[b]*Department of Environmental Engineering, College of Engineering, University of Baghdad, Baghdad, Iraq, email: Ahmed.abedm@yahoo.com*

Received 22 August 2022; Accepted 27 December 2022

ABSTRACT

This work has proposed a preparation membranous shaped Cu-Al layered double hydroxide (LDH) based nanocomposites using a co-precipitation technique with bentonite incorporation. The prepared bentonite-supported CuAl-LDH (B-CuAl) structures and morphology were identified by Fourier-transform infrared spectroscopy, X-ray diffraction and scanning electron microscopy. Furthermore, the regeneration capability and reuse of the prepared adsorbent have been investigated. The response surface methodology was applied to optimize the adsorption parameters and assess the interaction effects. The results revealed that the highest abamectin removal was 97.99%, at optimal conditions of pH = 8, 10 mg/L abamectin pesticide concentration, 10 g/L adsorbent dosage, 90 min contact time, 40°C temperature, 250 μm particle size, and 300 rpm shaking speed. A second-order polynomial model was fitted to predict the adsorption yield of abamectin pesticide on the sum of squares, *P*-value, and *F*-value of the model obtained from analysis of variance results, which confirms a successful correction with the obtained data (R^2 = 99.97%, $R^2_{adj.}$ = 99.64%, and $R^2_{pred.}$ = 96.51%). This work demonstrates the potentials of environmental applications of bentonite supported LDH as an efficient adsorbent's removal of pesticides contaminants from aqueous solutions.

Keywords: Abamectin; Adsorption; B-CuAl; Co-precipitation; Morphology; Optimization

1. Introduction

Anthropogenic behaviors and industrial outputs are increasing the number of pollutants in the natural environment [1]. Pharmaceuticals (hormones, antibiotics, and others), cosmetics, synthetic dyes, and pesticides are among the pollutants that are causing great concern in many parts of the world [2]. Abamectin pesticide (ABM), an analogue of ivermectin is a novel insecticide generated from the fermentation of an actinomycete called *Streptomyces avermitilis*, it is also widely utilized active component that is employed not only in agriculture but also in medicines for both human and animal protection, however it can cause unconsciousness, acidosis, hypotension, and even death in extreme cases of overdose [3]. Because of ABM slow disintegration and lipophilic nature, its residues can infiltrate aquatic habitats via runoff or drift and accumulate in fish and aquatic bodies after use in agriculture [4].

The removal of pesticides from contaminated wastewater is a paramount issue and that's led to use various methods including iron-enhanced sand filters (IESFs) [5], chlorination [6], advanced oxidation processes [7], adsorption and biological treatment techniques [8]. Among them, adsorption is one of the most effective and economic method to sequestrate pesticides from wastewater due to

* Corresponding author.

easy operation, high efficiency, and easy recovery or reuse of adsorbent [9]. Adsorption efficacy is highly dependent on adsorbent characteristics thus; adsorbents with high surface area and more binding sites are required. Currently, many adsorbents have been investigated to remove pesticides from wastewater such as clay [10], zeolite [11], active carbon [12], graphitic carbon [13], biochar [14,15], and layered double hydroxide [16,17].

Layered double hydroxide (LDH) is a layered substance composed of divalent and trivalent metal ions from layers with anion interlayer space. The anion on the interlayer space can be exchanged based on the synthetic situation and application goal. Sulfate, carbonate, hydroxide, nitrate, chloride, and polyoxometalate are the most prevalent anion on interlayer LDH [18]. The general chemical composition can be written as $[M^{2+}_{(1-x)}M^{3+}x(OH)_2]x^+[A^{n-}]^{x/n}.mH_2O$ where M^{3+} and M^{2+} are trivalent and divalent metal ions, respectively, A^{n-} is the interlayer anion which balances the charge, and x is represented the ratio of $M^{3+}/(M^{3+} + M^{2+})$ [19]. LDHs and their calcined derivatives have been extensively researched as water pollutant adsorbents in recent years [20] due to their numerous properties like interlayer anion-exchange capacity, large surface area, and a positive charge on the surface. These characteristics make them good adsorbents for organic/inorganic contaminants, particularly their negatively charged species [21]. Recently, LDHs-based nanocomposites such as those hybridized with carbon materials, anions or polymers have been increasingly investigated for the removal of many types of hazardous pollutants from aqueous solution. These nanocomposites exhibit mixed qualities of parental material which resulted in improvement in surface area, excellent selectivity, and higher anion exchangeability [22].

Response surface methodology (RSM) based on a central composite design (CCD) has been utilized as a powerful and valuable method for modeling and optimizing a variety of processes [23]. Using experimental data, this model develops a functional link between the input parameter and the output response. RSM is a combination of analytical models that can be used to design experiments, develop processes, and optimize them to produce the desired outcome [24]. The RSM was applied as a systematic experimental design in many types of research such as the optimization of sulfate and nitrate removal using magnetic multi-walled carbon nanotubes [25,26]. In addition, many researchers used RSM to model the experimental pesticide adsorption in an aqueous solution by various adsorbents such as eggshell powder [27], GO/ZIF-8 [28], graphene oxide [29], activated carbon [30] and porous pumice [31]. A typical RSM design known as the Box–Wilson central composite design is appropriate for optimizing significant parameters such as pH, contact time, adsorbent dosage, agitation speed, particle size, initial ABM concentration, and temperature with a minimum number of tests, as well as analyzing the interaction between these variables. Based on our knowledge, there has been no work investigating the ability to use bentonite-supported CuAl-LDH (B-CuAl) synthesized by a co-precipitation method for the adsorption of pesticides from aqueous solution. Scanning electron microscopy (SEM), X-ray diffraction (XRD), and Fourier-transform infrared spectroscopy (FTIR) were used to characterize this novel adsorbent.

2. Experimental

2.1. Adsorbate

Abamectin pesticides were used as adsorbate. A stock solution (1,000 mg/L) was prepared and diluted appropriately. The concentration of abamectin was determined by ultraviolet-visible (UV) spectrophotometer (PG Instruments, Model T80 Double Beam, UK) at a wavelength of 210 nm. The structure of ABM is shown in Fig. 1.

2.2. Adsorbent

Bentonite incorporation with CuAl/LDH was synthesized by the coprecipitation technique according to [22,32] with slight modification. First about 50 mL of 0.5 M of divalent cation $Cu(NO_3)_2{\cdot}3H_2O$ with 50 mL of 0.250 M trivalent cation of $AL(NO_3)_3{\cdot}9H_2O$ mixed in deionized water under constant stirring for 1 h until the starting materials dissolved. At that point, 3 g of bentonite in 60 mL of deionized water was stirred for 1 h before being added to the reaction flask of divalent and trivalent salts. Subsequently, a solution of 1 M sodium hydroxide was added dropwise to achieve pH 10 ± 0.5 while keeping the stirring speed maintained for a few hours, this NaOH solution acted as a precipitating agent [33]. The composite was separated by filtration and washed thoroughly with deionized water to purify the LDH until the pH was 7 and then dried at 60°C overnight [34].

2.3. Characterization of B-CuAl LDH

The B-CuAl was characterized using several techniques. The structures of the adsorbent were analyzed at room temperature by X-ray Diffractometer (Philips PW 1730/10) (XRD) with a copper anode of (λ = 1.5406 Å) radiation, FTIR spectroscopic test made in (Shimadzu, Japan) was investigated to detect the surface, functional groups of the analyzed adsorbents, at a wavenumber of 400–4,000 cm^{-1} and scanning electron microscopy by (TESCAN Mira3, 10 kV) SEM at various magnifications was used to evaluate surface morphology and shape changes.

2.4. Response surface methodology

In this study, RSM and historical data design using Design-Expert V13 were employed to optimize the following

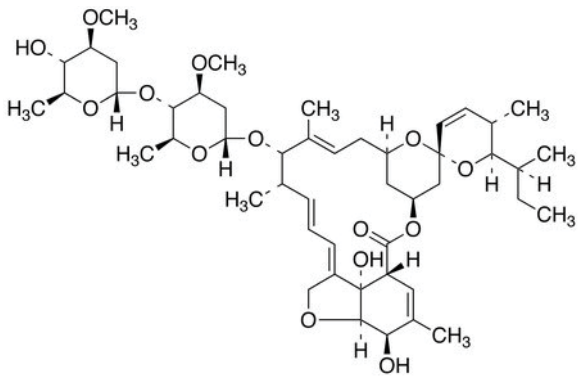

Fig. 1. Chemical structure of abamectin.

seven parameters: initial ABM concentration, shaking speed, pH, adsorbent dose, temperature, particle size, and contact time as independent variables, these seven variables were chosen. The output response variable was set to the percentage of ABM removed (%).

Table 1 displays the variables, ranges, and levels. The cumulative influence of these seven factors was studied using the central composite design (CCD). Eq. (1) was fitted to the quadratic response surface model [35]:

$$y = \beta_0 + \sum_{i=1}^{k} \beta_i x_i + \sum_{i=1}^{k} \beta_{ii} x_i^2 + \sum_{1 \le i \le j}^{k} \beta_{ij} x_i x_j + \varepsilon \quad (1)$$

where Y is the predicted response; β_0 is the constant coefficient, β_i is the linear coefficient, β_{ii} is the quadratic coefficient, β_{ij} is the interactive coefficient; x_i, x_i^2, and x_j are independent factor values in coded units, and ε = the model's error. The response is graphically depicted by contour plots and surface plots, which highlight the interaction effects between the fundamental precepts and optimum system conditions. Analysis of variance (ANOVA) was used to evaluate the statistically significant results of the quadratic model and all of its related model terms. *P*-values less than 0.005 are considered statistically significant. The data was analyzed using design expert software, the experimental data was added, and the interaction impact of independent factors on the response was optimized. This approach allows us to determine the effect of various processing parameters on adsorption with a limited number of experiments.

3. Results and discussion

3.1. Characterization of adsorbent

The FTIR spectroscopic analysis of the B-CuAl with mole ratio 2:1 before and after ABM adsorption, are shown in Fig. 2a and b and the analysis of the B-CuAl with mole ratio 4:1 before and after ABM adsorption, are shown in Fig. 2c and d. Fig. 2a and c show the stretching vibration related to the Si–O–Al bond due to bentonite being centered at almost 1,000 cm^{-1} [32], the stretching mode of the OH group is detected as a broad band between 3,000 and 3,500 cm^{-1} in the wide peak for B-CuAl LDH [36,37], the peaks at 1,534 cm^{-1} could be recognized to N–N stretching vibrations [38], bands 1,388 cm^{-1} are related with the stretching vibrations of the NO_3^- ions group [33]. Bands in the 500–800 cm^{-1} region are associated with Cu–O, Al–O, and metal-oxygen bonds in a brucite-type layer [39]. Fig. 2b shows the FTIR spectra for B-CuAl after adsorption. After ABM adsorption, the O–H peak of B-CuAl changed from 3,251 to 3,244 cm^{-1}, indicating that hydrogen bonding, formed by surface O–H of B-CuAl and ABM, may have contributed to the adsorption process [39] while in Fig. 2d the O–H changed from 3,383.147 to 3,383.157 cm^{-1}. New peaks were mostly seen in the range 3,251–1,006 cm^{-1} after ABM adsorption. As a result, the effective removal of the ABM under consideration may be identified with the assistance of the aforementioned functional groupings and a 2:1 ratio is more preferable than a 4:1 ratio for ABM removal.

The XRD obtained results of B-CuAl determined using two different ratios are shown in Fig. 3, the average diameter size of B-CuAl computed using Debye–Scherrer equation [39,40].

$$D = \frac{0.89\lambda}{b\cos\theta} \quad (2)$$

where D is the crystallite size, b is the full-width at half maximum (FWHM) in radians, λ is the wavelength of the incident X-rays = 0.154 nm and θ is the half diffracted Bragg angle of 2θ, the size of crystallite is a key element that plays a major impact in catalytic activity. Using Eq. (2), the diameters of B-CuAl with mole ratios (2:1, 4:1) were determined to be 16.45 and 22.04 nm, respectively.

Fig. 3a confirms the presence of diffraction reflections at intensities of 12.04°, 26.4°, 35.4°, 38.4°, 48.5°, 53.4°, 57.9°, and 61.2° which match the reflections 003, 006, 012, 009, 015, 018, 110, and 113, respectively while Fig. 3b confirms the presence of diffraction reflections at intensities of 26.7°, 35.6°, 38.5°, 48.8°, 53.7°, 58.1°, and 61.6° which match to the reflections 006, 012, 009, 015, 018, 110, and 113, respectively indicating that the materials have a layer structure [33]. The basal spacing of B-CuAl LDH with mole ratio 2:1 is 7.345 Å at 2θ = 12.04°, the (003) reflection, and it has a well-formed layered structure [42]. The reflections (003), which define the lamellar phase of LDHs, were not detected in the case of ratio 4:1. This absence is related to the copper ions' Jahn–Teller

Table 1
Experimental range and values of the independent variables

Designation	Data	Unit	Lower limit	Upper limit	Lower weight	Upper weight	Importance
Factor 1	Contact time	min	15	90	1	1	3
Factor 2	pH		4	9	1	1	3
Factor 3	Adsorbent dosage	g/L	1	10	1	1	3
Factor 4	Shaking speed	rpm	200	300	1	1	3
Factor 5	Temperature	°C	20	40	1	1	3
Factor 6	Initial concentration	mg/L	10	200	1	1	3
Factor 7	Particle size	μm	250	600	1	1	3
Response	Removal	%	0	98	1	1	3

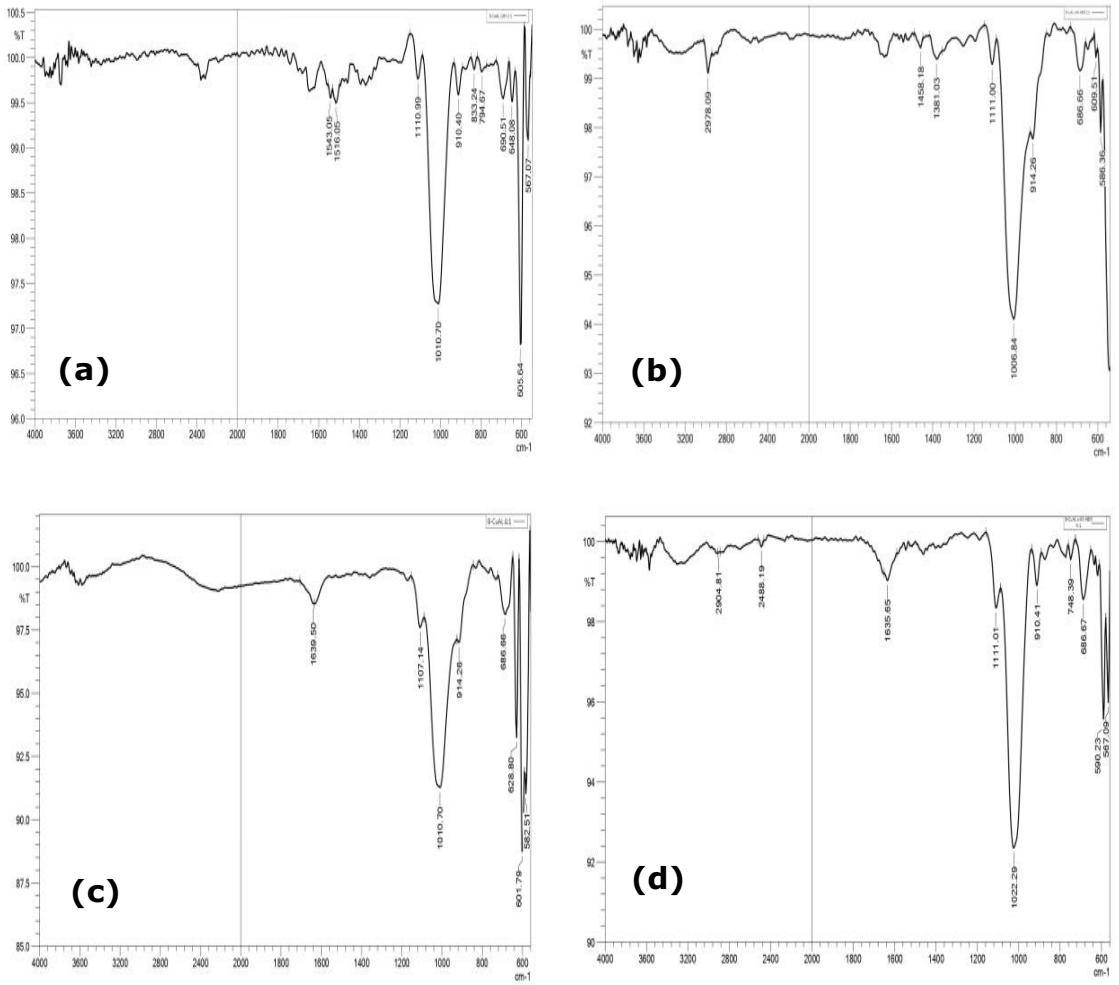

Fig. 2. FTIR spectra (a) for B-CuAl (2:1), (b) for B-CuAl after ABM adsorption (2:1), (c) for B-CuAl (4:1), and (d) for B-CuAl after ABM adsorption (4:1).

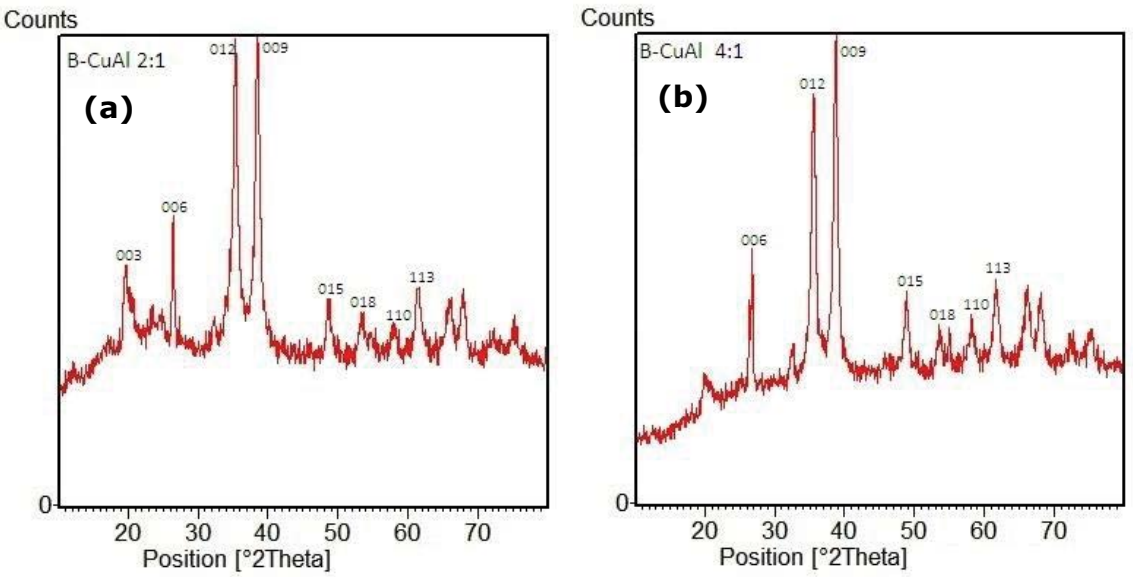

Fig. 3. XRD patterns (a) for B-CuAl (2:1) and (b) for B-CuAl (4:1).

effect [43]. This result shows that when the concentration of Cu^{2+} in the layer increases, the distortion caused by the Jahn-Teller effect decreases hydrogen bonding resulting in poor long-range ordering, as is frequently documented for copper-divalent LDH systems and this is in agreement with the information provided by [44]. Generally, peaks at 61.2° and 61.6° appeared as an anion phase on interlayer distance. Metal oxide build-up on layer structure is ascribed to diffraction peaks in the 20°–35° range [45]. These peaks also indicate a layered structure and reflect the hexagonal LDH, LDH typically takes on a hexagonal shape with an interlayer space that is entirely made up of anion interlayers and water molecules, the water molecules in the interlayer formed hydrogen-bonded with the anions and metal hydroxide layer [46]. Because of the presence of bentonite, the surface of the LDH has a broad peak at 26 [32].

Fig. 4 shows the SEM image of B-CuAl with mole ratio 2:1 and 4:1 before and after interaction with ABM, Fig. 4a and c depict the creation of a plate-like layer for coated bentonite, which was composed of roughly aggregated micrometric plates with uneven orientations and sizes, and a high surface-to-volume ratio. Typically increasing the surface area subjected to contaminant interaction can enhance adsorbent efficiency. The particle size distribution is determined by the synthesis conditions and ranges in lateral dimensions from a few hundred nm to a few μm [47]. As a result of the binding of ABM molecules with sorbent after the sorption process, the sorbent morphology was noticeably changed Fig. 4b and d in contrast to sorbent before contact with ABM and characterized by grooved lumped with considerable residues of whitish color pollutants sorbed that virtually covered the sorbent surface.

3.2. Regeneration

Regeneration of used LDH is essential in both economic and environmental aspects [22]. Many adsorption–desorption cycles were performed sequentially to test the feasibility of the ABM removal procedure. The regeneration method depends on the desorption of ABM from the exhausted sorbent. It consisted of extracting the LDH from the aqueous solution through filtering, washing it multiple times with distilled water, repeating it with 0.5 M HCl as an eluent agent, and drying it in an oven at 60°C until total dryness. The adsorption was carried out under the following conditions: pH = 8, C_o = 50 mg/L, time = 60 min, agitation speed = 300 rpm, and adsorbent dosage = 4 g/L.

This technique was investigated by repeating the desorption procedure for five cycles, and the percentage of ABM recovered was measured for each cycle. Fig. 5 clearly shows

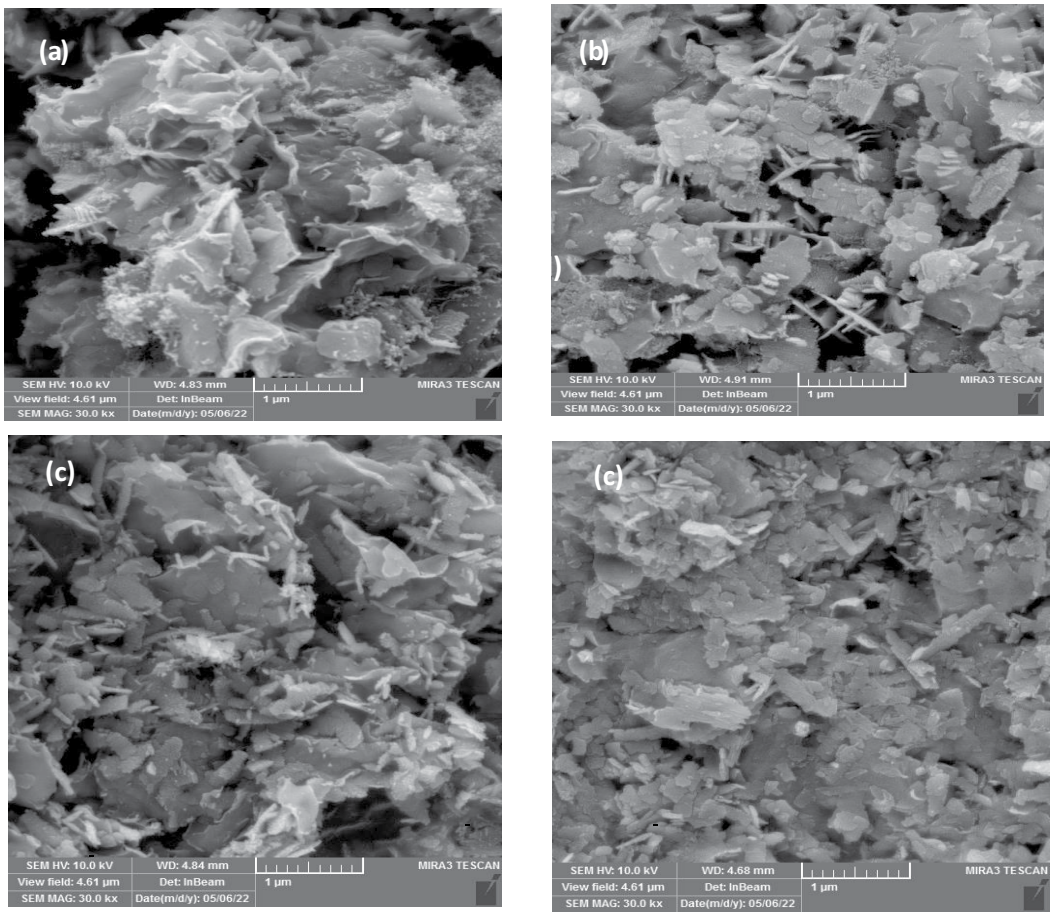

Fig. 4. SEM graphs magnification scale of 1 μm. (a) For B-CuAl (2:1), (b) for B-CuAl after ABM adsorption (2:1), (c) for B-CuAl (4:1), and (d) for B-CuAl after ABM adsorption (4:1).

that the sorption effectiveness was 86.32%, 84.12%, 65.06%, 40.1%, and 32.3% for the first, second, third, fourth, and fifth cycles, respectively.

Since B-CuAl LDH dissolves in the acidic reagent and cannot be reused, its efficiency was lowest after the fourth regeneration. According to Nishimura et al. [48], LDHs treated in regeneration procedures may suffer structural damage owing to exfoliation. However, the synthesized sorbent in this study had acceptable recyclability, indicating that it may be a promising choice to serve as an effective and sustainable adsorbent for ABM sorption.

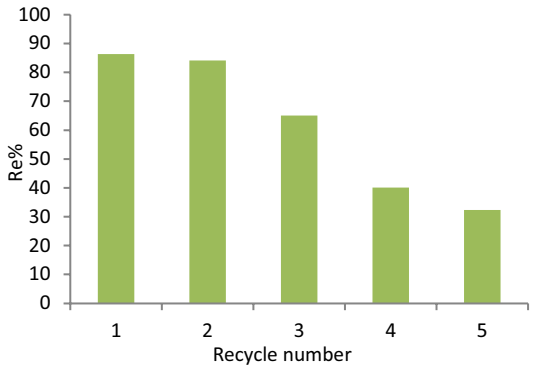

Fig. 5. Removals of ABM using B-CuAl LDH in the recycle tests (W = 4 g/L; T = 25°C; C_i = 50 mg/L; pH = 8; rpm = 300; time = 60 min).

3.3. Representation of optimization

RSM was used to investigate the simple and interactive impacts of operational variables on ABM removal. The optimization design method, based on the central composite, consists of the following key steps: carry out statistically planned experiments in line with the experimental strategy, suggest a mathematical model derived from empirical data and analyze the variance result, predict the response and verify the model [30]. Table 2 displays the findings of trials in the form of ABM removal percentages from aqueous solutions that were evaluated using the CCD. The application of RSM's historical data design resulted in a regression model for the response of ABM removal (%). A second-order polynomial model was chosen based on the sum of squares, P-value, and F-value of the model obtained from ANOVA results [49]. Eq. (3) depicts the second-order polynomial (quadratic) equation produced from CCD in terms of actual factors.

$$\begin{aligned}\text{ABM removal} = {} & 24.72863 + 0.417360A \\ & + 87.27435B - 1050.19783C + 2.78389D \\ & - 49.02719E + 4.09863F + 1.03681G \\ & - 0.270373AB + 1.52248AC - 0.006081AD \\ & + 0.166378AE - 0.013297AF - 0.003691AG \\ & + 36.21267BC - 0.2534BD + 1.48378BE \\ & - 0.357534BF - 0.007307BG + 1.65989CD \\ & - 1.6366CE - 0.322556CF + 0.934653CG \\ & + 0.044885DE + 0.010390DF - 0.009065DG \\ & - 0.055904EF + 0.047819EG - 0.003653FG \\ & - 0.002117A^2 - 3.27641B^2 + 1.09837C^2 \\ & - 0.000711D^2 + 0.114224E^2 - 0.000696F^2 \\ & - 0.000102G^2 \end{aligned} \quad (3)$$

According to the equation, when the pesticide concentration increased, the removal decreased, but increasing the adsorbent dosage improved the removal. Fig. 6 depicts the Pareto chart, it can be noticed that factors A, B, C, and D (orange bar) which represented contact time, pH, adsorbent dosage, and shaking speed, respectively have a synergistic influence while F and G (blue bars) which represented particle size and initial concentration, respectively have an antagonistic influence on the B-CuAl LDH adsorption capacity. The adsorbent dosage and initial concentration have the greatest impact on the adsorption process. Fig. 7 shows the predicted vs. actual ABM removal percentages. The results show that the points in this figure have good relationships and most of the 39 data points landed on the parity diagonal, indicating that the model is accurate for the intended purpose.

3.4. Statistical analysis

The ANOVA determines the model's adequacy; Table 3 displays the results of the ANOVA for pesticide removal, the variance of the independent parameters predicted by the correlation/model is represented by the R^2 value, the better the model; the closer R^2 is to 1 [50]. The findings reveal that the regression was statistically significant for ABM, with an F-value of 305.48. R^2 and adjusted R^2 values for the new model were 0.9997 and 0.9964, respectively. Given that 39 lines of data, so high dependability are remarkable, it is quite remarkable to obtain such high coefficient of determination values while analyzing a large set of data. This is a measure of how accurate the model is in predicting the statistical significance of the components, this test is important to show if the model has not been adequately fitted [51]. The change in data surrounding the fitted model is described by the lack of fit tests. The lack of fit F-value is 0.04 indicating that the lack of fit is not significant in comparison to the pure error, confirming the model's data fitness. Furthermore, Table 3 reveals that the Adeq. Precision ratio was 47.3948%, indicating a sufficient signal. Adeq. Precision evaluates the signal-to-noise ratio and is preferable at a ratio > 4 [52].

3.5. Response surface plots for ABM residue removal

To obtain an understanding of the interactions between variables and validate the optimal level of each variable to a maximum adsorption value, three-dimensional (3D) response surface plots and two-dimensional (2D) contour plot illustrations of the response surface of the adsorbed amount of ABM relative to the seven variables were used [53]. RSM contour plots are generated as a function of two variables at a time, with all other variables held constant [51]. It is possible to construct a link between the significant parameters during contaminant adsorption from Fig. 8

Table 2
Experiment results according to central composite design

Std.	Run	Factor 1	Factor 2	Factor 3	Factor 4	Factor 5	Factor 6	Factor 7
		A: Contact time	*B*: pH	*C*: Adsorbent dosage	*D*: Shaking speed	*E*: Temperature	*F*: initial concentration	*G*: particle size
31	1	52.5	6.5	5.5	250	20	105	425
12	2	90	9	10	200	40	10	250
34	3	52.5	6.5	5.5	250	30	200	425
1	4	90	9	10	200	40	200	600
36	5	52.5	6.5	5.5	250	30	105	600
9	6	90	4	10	200	20	10	600
8	7	90	9	10	300	20	200	250
26	8	52.5	9	5.5	250	30	105	425
35	9	52.5	6.5	5.5	250	30	105	250
18	10	90	4	1	300	40	200	600
4	11	90	4	10	300	20	200	600
3	12	90	9	1	300	40	10	600
24	13	90	6.5	5.5	250	30	105	425
25	14	52.5	4	5.5	250	30	105	425
20	15	15	4	10	300	40	200	250
23	16	15	6.5	5.5	250	30	105	425
11	17	15	9	1	300	20	10	250
5	18	15	9	10	200	20	200	250
29	19	52.5	6.5	5.5	200	30	105	425
38	20	52.5	6.5	5.5	250	30	105	425
2	21	90	9	1	300	20	200	250
7	22	15	9	1	300	40	10	600
28	23	52.5	6.5	10	250	30	105	425
37	24	52.5	6.5	5.5	250	30	105	425
39	25	52.5	6.5	5.5	250	30	105	425
21	26	15	9	10	300	20	10	600
33	27	52.5	6.5	5.5	250	30	10	425
22	28	15	4	1	200	20	10	250
16	29	90	4	1	200	20	200	600
14	30	15	4	10	200	20	10	600
10	31	15	4	1	200	40	200	250
27	32	52.5	6.5	1	250	30	105	425
13	33	90	4	1	300	20	10	250
19	34	15	4	10	300	40	10	600
17	35	15	9	1	200	40	200	600
32	36	52.5	6.5	5.5	250	40	105	425
30	37	52.5	6.5	5.5	300	30	105	425
6	38	90	4	1	200	40	10	250
15	39	15	9	1	200	20	200	600

shows surface plots of ABM removal % with pH, shaking speed, contact time, adsorbent dose, temperature, initial concentration, and particle size. Fig. 8a shows the influence of initial concentration, and adsorbent dose on ABM adsorption while keeping contact time, pH and temperature constant at 60 min, 8, and 25°C, respectively, this figure clearly shows that B-CuAl LDH dose and ABM initial concentration were the most important factors influencing the response and the results showed that the greatest adsorption occurred in the adsorbent dosage 4 g/L and at low initial ABM concentrations, the capacity of the adsorbent to remove ABM from the solution is determined by the adsorbent dosage, whereas ABM initial concentration has a significant impact on the mass transfer barrier between both the aqueous and solid phases [54]. Fig. 8b shows the influence of adsorbent dose and pH on ABM adsorption while keeping the initial ABM

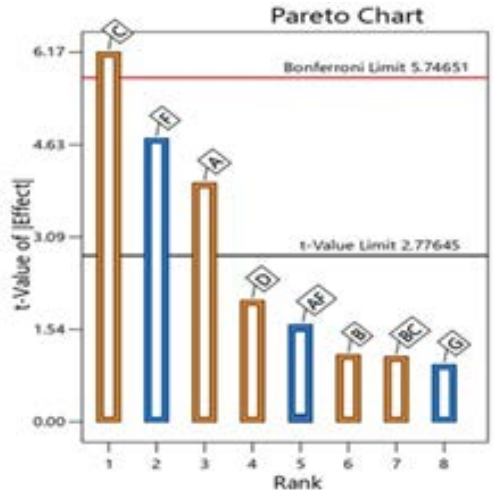

Fig. 6. Pareto chart.

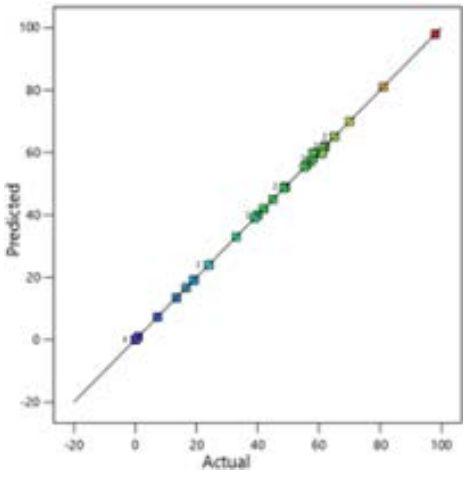

Fig. 7. Actual vs. predicted values.

concentration constant at 50 mg/L, the temperature at 25°C and contact time at 60 min, the data confirmed that the highest removal efficiency of ABM was shown under alkaline conditions, and the removal of ABM increases with increasing pH from 4 to 9. This can be related to the surface charge and the existence of binding sites on the composite surface, a feature that is mostly associated with the LDH, thus the negative charge on the surface of these materials, making ABM more likely to be absorbed [41]. Fig. 8c shows the influence of particle size and initial concentration while holding other parameters constant; the study discovered that as particle size reduced, ABM removal efficiency increased and this is attributed to that smaller particle size s provide larger surface areas, which allow for faster adsorption [55,56]. Fig. 8d depicts the combined impact of adsorbent dose and shaking speed, the data suggest that ABM removal increases as agitation speed increases at a given time. This is most likely owing to improved contact between the adsorbent and adsorbate at greater speeds [57]. Fig. 8e represents the combined effect of contact time and initial concentration, contact time plays an important role in the adsorption of ABM pesticide by B-CuAl LDH adsorbent, the amount of ABM removed increased rapidly in the early time before reaching the equilibrium level after 60 min, this might be attributed to the presence of a significant number of available active sorbent in the initial contact time, as well as the accelerated rate of transfer of ABM molecules from the solution to the surface of the adsorbent [58]. Fig. 8f depicts the influence of contact time and adsorbent dose on ABM adsorption when other parameters remain constant. The results reveal that the ABM removal rate was greater within the first 30 min, after that, the increase in contact time resulted in a slower ABM adsorption rate [59]. Fig. 8g depicts the influence of temperature and initial ABM concentration; the results demonstrate that raising the adsorption process temperature improves LDH adsorption capacity, This is related to increased contaminant mobility in aqueous solution, which enhances adsorption site accessibility [22].

A comparison of the impacts of all variables on ABM removal efficiency was assessed by perturbation plot in Fig. 9. The steep lines in B-CuAl dosage (*C*), ABM initial concentration (*F*), and pH (*B*) in the figure demonstrate that the response of ABM removal efficiency was highly affected by these parameters. ABM removal efficiency was 86.32% at B-CuAl dosage 4 g/L, ABM initial concentration 50 mg/L, pH 8, temperature 40°C, contact time 60 min, shaking speed 300 rpm, and particle size 250 μm.

3.6. Optimization conditions

For multivariate problems, numerical optimization has shown to be an extremely useful tool. This is due to the complexities involved in determining optimal operating points, which required data analysis of all independent and dependent variables at a time [60]. To achieve maximal ABM removal from wastewater, the optimal values of independent variables such as pH, ABM initial concentration, contact time, adsorbent dose, temperature, shaking speed, and particle size were determined. The goals are combined to create a desirability function. The software is investigating ways to improve this functionality; the application is looking into this capability. The goal-finding procedure begins at random and proceeds up the sharpest slope to the highest peak [61]. At the following condition, the optimal parameters for 97.99% ABM removal were obtained: 9 as pH, 10 mg/L ABM concentrations, 10 g/L adsorbent dosage (B-CuAl LDH), 90 min contact time, 40°C temperature, 250 μm particle size, and 300 rpm shaking speed, the desired profile response s for ABM removal % using B-CuAl LDH adsorbent depicted in Fig. 10. Table 4 compares some experimental optimal data for pesticide adsorption by several adsorbents using RSM. From Table 4 it can be noticed that the experimental results demonstrated that different types of adsorbents may successfully increase the removal of various types of pesticides by up to about 100%. The variances in performance can be attributed to the various characteristics of adsorbents, the quantity of utilized adsorbents, pesticide types, pH, pesticide initial concentration, shaking speed, contact time, and temperature. This finding suggests that the B-CuAl LDH has significant adsorption properties, implying that it might be beneficial in pesticide removal from aqueous solutions.

Table 3
ANOVA for response surface quadratic model of B-CuAl

Source	Sum of squares	df	Mean square	*F*-value	*P*-value	
Model	21,821.93	35	623.48	305.48	0.0003	Significant
A: Contact time	134.48	1	134.48	65.89	0.0039	
B: pH	1,030.58	1	1,030.58	504.93	0.0002	
C: Adsorbent dosage	8	1	8	3.92	0.1421	
D: Shaking speed	8	1	8	3.92	0.1421	
E: Temperature	192.08	1	192.08	94.11	0.0023	
F: Initial concentration	264.5	1	264.5	129.59	0.0015	
G: Particle size	3.65	1	3.65	1.79	0.2737	
AB	539.64	1	539.64	264.4	0.0005	
AC	1,827.89	1	1,827.89	895.57	<0.0001	
AD	248.17	1	248.17	121.59	0.0016	
AE	1,648.69	1	1,648.69	807.78	<0.0001	
AF	1,173.78	1	1,173.78	575.09	0.0002	
AG	523.74	1	523.74	256.61	0.0005	
BC	807.11	1	807.11	395.44	0.0003	
BD	433.86	1	433.86	212.57	0.0007	
BE	1,263.85	1	1,263.85	619.22	0.0001	
BF	686.43	1	686.43	336.32	0.0004	
BG	12.27	1	12.27	6.01	0.0915	
CD	675.27	1	675.27	330.85	0.0004	
CE	23.17	1	23.17	11.35	0.0434	
CF	169.95	1	169.95	83.27	0.0028	
CG	509.24	1	509.24	249.5	0.0006	
DE	162.98	1	162.98	79.85	0.003	
DF	1,268.74	1	1,268.74	621.62	0.0001	
DG	695.17	1	695.17	340.6	0.0003	
EF	575.3	1	575.3	281.87	0.0005	
EG	875.76	1	875.76	429.08	0.0002	
FG	1,078.39	1	1,078.39	528.36	0.0002	
A^2	20.55	1	20.55	10.07	0.0504	
B^2	972.1	1	972.1	476.28	0.0002	
C^2	0.1147	1	0.1147	0.0562	0.8279	
D^2	7.33	1	7.33	3.59	0.1545	
E^2	302.46	1	302.46	148.19	0.0012	
F^2	91.36	1	91.36	44.76	0.0068	
G^2	22.68	1	22.68	11.11	0.0446	
Residual	6.12	3	2.04			
Lack of fit	0.1231	1	0.1231	0.041	0.8582	Not significant
Pure error	6	2	3			
Cor. total	21,828.05	38				
Response of quadratic	R^2	$R^2_{adj.}$	$R^2_{pred.}$	Std. Dev.	C.V. (%)	Adeq. precision
summary statistics	0.9997	0.9964	0.9651	1.43	3.28	47.3948

4. Conclusions

In the present work, CuAl layered double hydroxide (LDH) based nanocomposite was produced using a co-precipitation technique with bentonite incorporation to prepare a high specific surface area bentonite supported CuAl LDH (B-CuAl). The synthesized B-CuAl was characterized using XRD, FTIR, and SEM to investigate its ability to eliminate abamectin pesticides from wastewater. ABM removal was modeled using the RSM-CCD framework involving Box–Behnken design based on seven independent variables, and the interaction impacts of these process variables on the removal efficiency were investigated. A high ABM removal efficiency (97.99%) was obtained at the optimum conditions

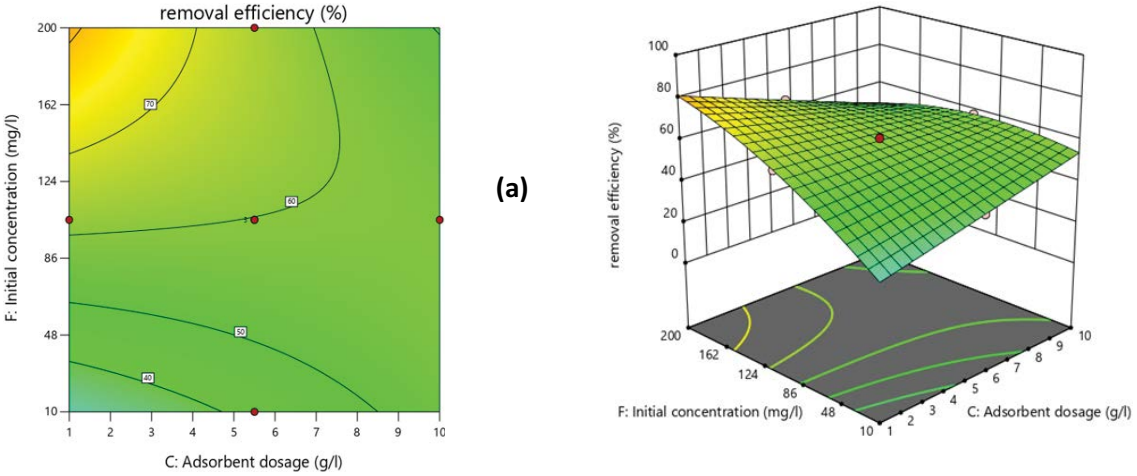

(a)

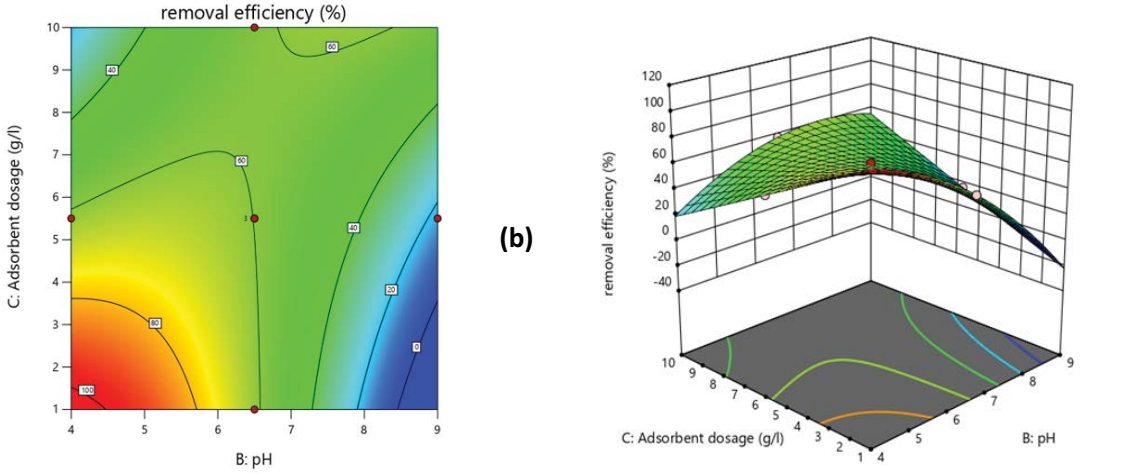

(b)

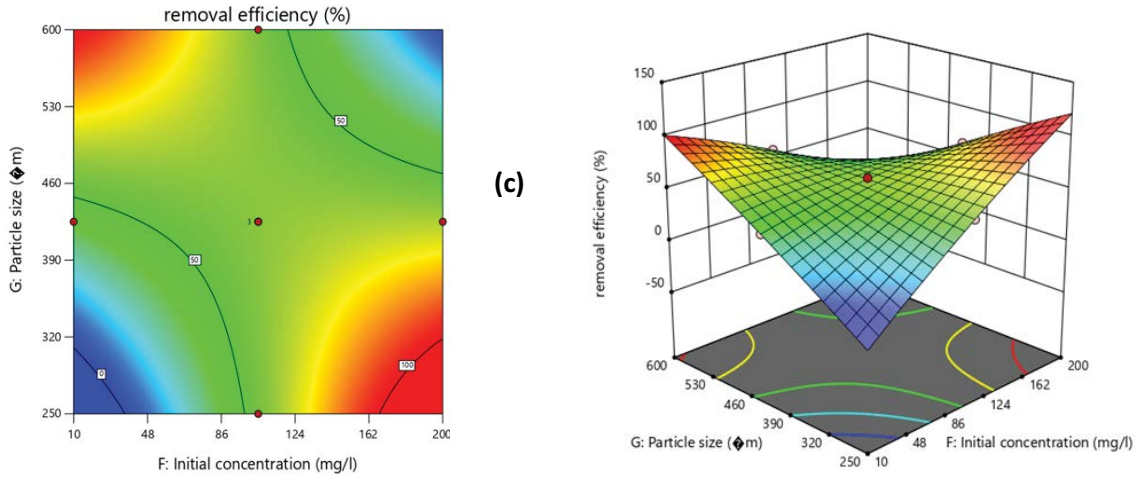

(c)

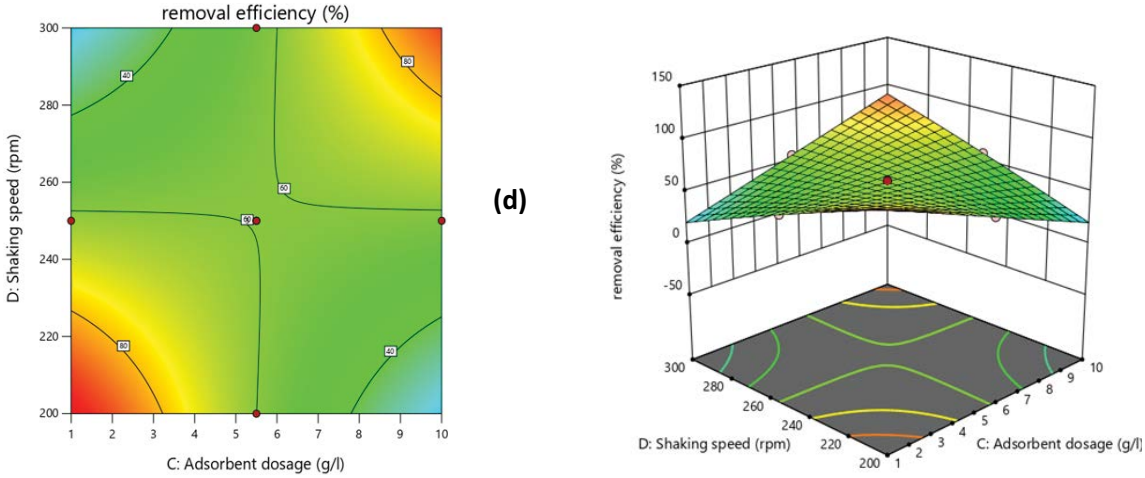

(d)

Fig. 8. (Continued)

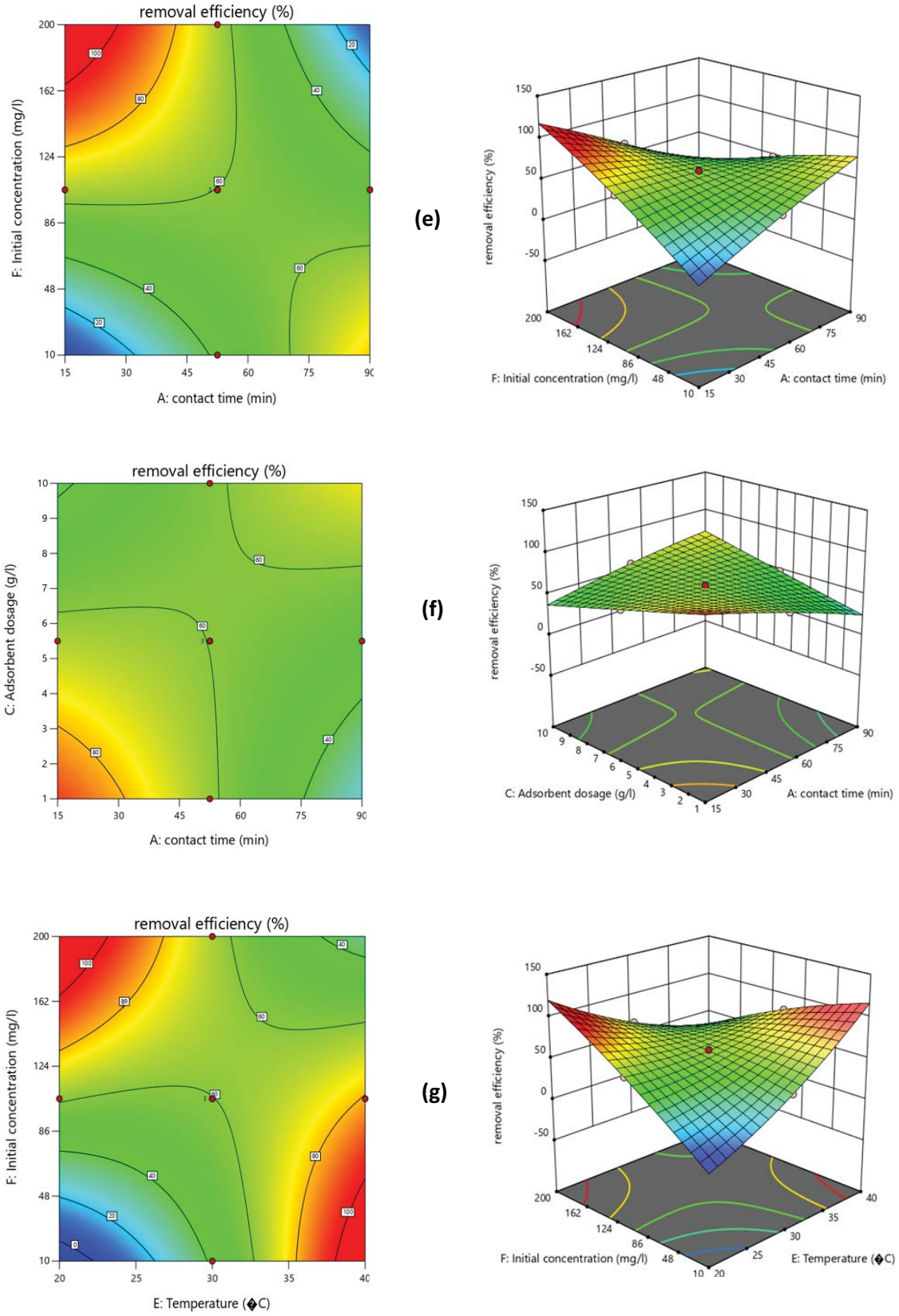

Fig. 8. 2D–3D surface plots of the interactive impact variables.

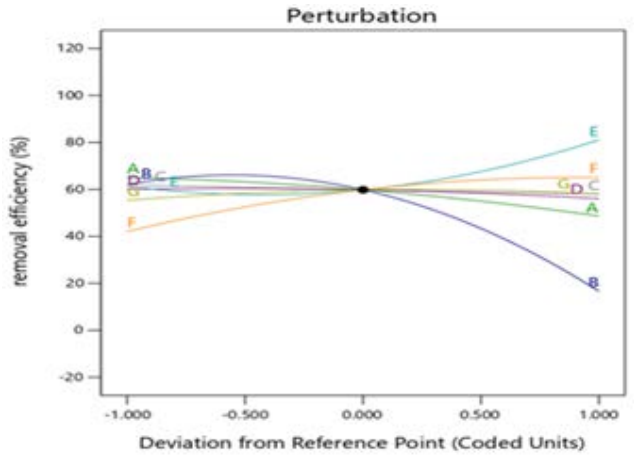

Fig .9. Perturbation plot for ABM removal.

pH = 9, ABM initial concentration = 10 mg/L, adsorbent dosage = 10 g/L, contact time = 90 min, temperature = 40°C, particle size = 250 μm and shaking speed = 300 rpm. ANOVA indicated a coefficient of determination (R^2 = 99.97%, $R^2_{adj.}$ = 99.64%, and $R^2_{pred.}$ = 96.51%) which was quite remarkable for 39 lines of data. According to the sum of squares, *P*-value, and *F*-value of the model derived from ANOVA results, a second-order polynomial model could be adequately fitted to the experimental data. Based on these findings, the B-CuAl LDH nanocomposite has potential applications in ABM adsorption. Also, it can be easily regenerated by 0.5 HCL and successfully used for several cycles.

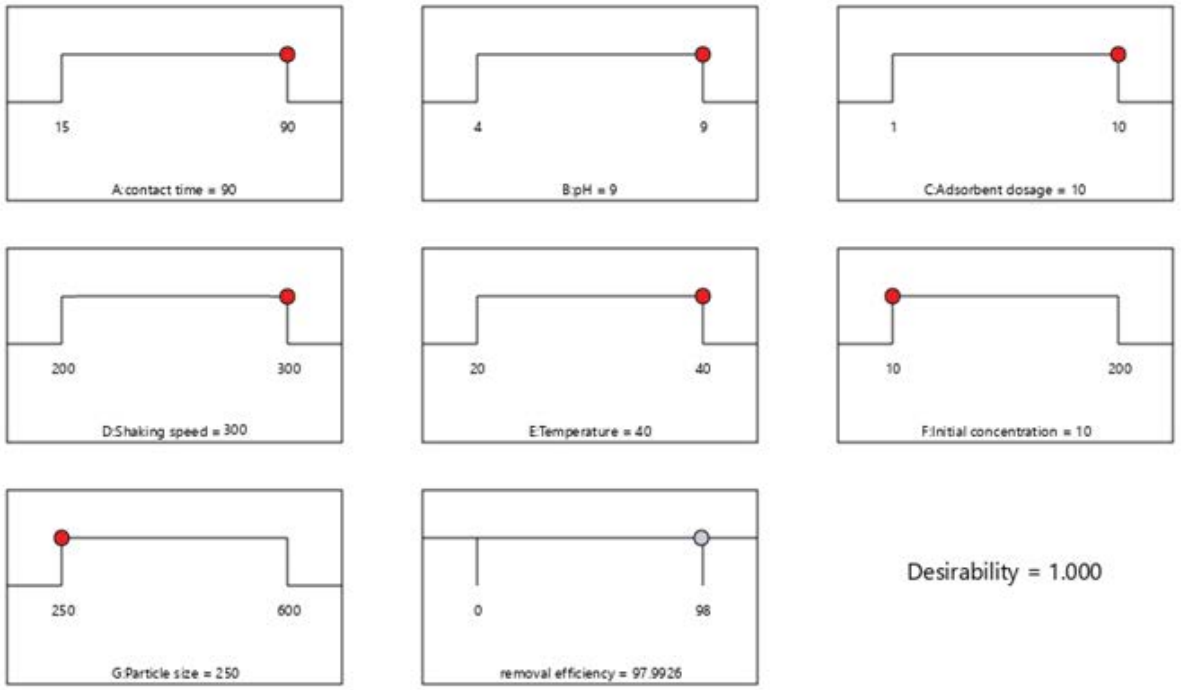

Fig. 10. Predicted response's desirability graphs.

Table 4
Comparison of some experimental optimum data by several adsorbents for pesticides adsorption

Adsorbent	Adsorbent dose (g/L)	Pesticides initial concentration (mg/L)	pH	Contact time (min)	Re (%)	References
B-CuAl LDH	10	10	9	90	97.99	This work
GO/Clay/Fe_3O_4	1.24	1.45	7	16	99.85	[62]
Activated carbons	1	100	9	120	96.05	[30]
Pumice	4	6.2	3	30	76.3	[31]
Chestnut shells	60	75	2	40	84.48	[63]
Egg-shell powder	1	24.4	2	5	92.2	[27]
Neem bark dust	1	12.38	5.51	–	99.74	[64]
Sodalite zeolite	3	50	6	80	63.4	[65]

References

[1] N.H. Arihilam, E.C. Arihilam, Impact and control of anthropogenic pollution on the ecosystem – a review, J. Biosci. Biotechnol. Discov., 4 (2019) 54–59.

[2] L.A. de V. Gomes, A.L. Facin, M.S. Salerno, R.K. Ikenami, Unpacking the innovation ecosystem construct: evolution, gaps and trends, Technol. Forecasting Social Change, 136 (2018) 30–48.

[3] H. Aminiahidashti, S.R. Jamali, A.M. Gorji, Conservative care in successful treatment of abamectin poisoning, Toxicol. Int., 21 (2014) 322–324.

[4] H.K. Mahmoud, F.M. Reda, M. Alagawany, M.R. Farag, The stress of abamectin toxicity reduced water quality, growth performance, immunity and antioxidant capacity of *Oreochromis niloticus* fish: modulatory role of *Simmondsia chinensis* extract as a dietary supplement, Aquaculture, 534 (2021) 736247, doi: 10.1016/j.aquaculture.2020.736247.

[5] D.J. Fairbairn, S.M. Elliott, R.L. Kiesling, H.L. Schoenfuss, M.L. Ferrey, B.M. Westerhoff, Contaminants of emerging concern in urban stormwater: spatiotemporal patterns and removal by iron-enhanced sand filters (IESFs), Water Res., 145 (2018) 332–345.

[6] W. Li, R. Wu, J. Duan, C.P. Saint, J. van Leeuwen, Impact of prechlorination on organophosphorus pesticides during drinking water treatment: removal and transformation to toxic oxon byproducts, Water Res., 105 (2016) 1–10.

[7] M. Malakootian, A. Shahesmaeili, M. Faraji, H. Amiri, S. Silva Martinez, Advanced oxidation processes for the removal of organophosphorus pesticides in aqueous matrices: a systematic review and meta-analysis, Process Saf. Environ. Prot., 134 (2020) 292–307.

[8] I.A. Saleh, N. Zouari, M.A. Al-Ghouti, Removal of pesticides from water and wastewater: chemical, physical and biological treatment approaches, Environ. Technol. Innovation, 19 (2020) 101026, doi: 10.1016/j.eti.2020.101026.

[9] M.A. Al-Ghouti D.A. Da'ana, Guidelines for the use and interpretation of adsorption isotherm models: a review, J. Hazard. Mater., 393 (2019) 122383, doi: 10.1016/j.jhazmat.2020.122383.

[10] F.M. de Souza, O.A.A. dos Santos, M.G.A. Vieira, Adsorption of herbicide 2,4-D from aqueous solution using organo-modified bentonite clay, Environ. Sci. Pollut. Res., 26 (2019) 18329–18342.

[11] M. Andrunik, T. Bajda, Removal of pesticides from waters by adsorption: comparison between synthetic zeolites and mesoporous silica materials. A review, Materials (Basel), 14 (2021) 3532, doi: 10.3390/ma14133532.

[12] J.M. Salman, V.O. Njoku, B.H. Hameed, Adsorption of pesticides from aqueous solution onto banana stalk activated carbon, Chem. Eng. J., 174 (2011) 41–48.

[13] M. Khoshnood, S. Azizian, Adsorption of 2,4-dichlorophenoxyacetic acid pesticide by graphitic carbon nanostructures prepared from biomasses, J. Ind. Eng. Chem., 18 (2012) 1796–1800.

[14] H. Cederlund, E. Börjesson, D. Lundberg, J. Stenström, Adsorption of pesticides with different chemical properties to a wood biochar treated with heat and iron, Water Air Soil Pollut., 227 (2016) 11270–016.

[15] M. Essandoh, D. Wolgemuth, C.U. Pittman, D. Mohan, T. Mlsna, Adsorption of metribuzin from aqueous solution using magnetic and nonmagnetic sustainable low-cost biochar adsorbents, Environ. Sci. Pollut. Res., 24 (2017) 4577–4590.

[16] D. Chaara, I. Pavlovic, F. Bruna, M.A. Ulibarri, K. Draoui, C. Barriga, Removal of nitrophenol pesticides from aqueous solutions by layered double hydroxides and their calcined products, Appl. Clay Sci., 50 (2010) 292–298.

[17] Y. You, H. Zhao, G.F. Vance, Adsorption of dicamba (3,6-dichloro-2-methoxy benzoic acid) in aqueous solution by calcined-layered double hydroxide, Appl. Clay Sci., 21 (2002) 217–226.

[18] A. Lesbani, P.M. Siregar, N.R. Palapa, T. Taher, F. Riyanti, Adsorptive removal methylene-blue using Zn/Al LDH modified rice husk biochar, Pol. J. Environ. Stud., 30 (2021) 3117–3124.

[19] S. Msamadya, Synthesis and Characterization of Layered Double Hydroxides and Their Application in Aspirin Intercalation, Masters Thesis, University of Zimbabwe, 2016.

[20] J. Cornejo, R. Celis, I. Pavlovic, M.A. Ulibarri, Interactions of pesticides with clays and layered double hydroxides: a review, Clay Miner., 43 (2008) 155–175.

[21] A. Nait-Merzoug, O. Guellati, S. Djaber, N. Habib, A. Harat, J. El-Haskouri, D. Begin, M. Guerioune, Ni/Zn layered double hydroxide (LDH) micro/nanosystems and their azorubine adsorption performance, Appl. Sci., 11 (2021) 8899, doi: 10.3390/app11198899.

[22] M. Zubair, M. Daud, G. McKay, F. Shehzad, M.A. Al-Harthi, Recent progress in layered double hydroxides (LDH)-containing hybrids as adsorbents for water remediation, Appl. Clay Sci., 143 (2017) 279–292.

[23] A.F. Abbas, M.J. Ahmed, Optimization of activated carbon preparation from date stones by microwave assisted K_2CO_3 activation, Iraqi J. Chem. Pet. Eng., 15 (2014) 33–42.

[24] N. Taoufik, A. Elmchaouri, S. El Mahmoudi, S.A. Korili, A. Gil, Comparative analysis study by response surface methodology and artificial neural network on salicylic acid adsorption optimization using activated carbon, Environ. Nanotechnol. Monit. Manage., 15 (2021) 100448, doi: 10.1016/j.enmm.2021.100448.

[25] V. Alimohammadi, M. Sedighi, E. Jabbari, Response surface modeling and optimization of nitrate removal from aqueous solutions using magnetic multi-walled carbon nanotubes, J. Environ. Chem. Eng., 4 (2016) 4525–4535.

[26] V. Alimohammadi, M. Sedighi, E. Jabbari, Optimization of sulfate removal from wastewater using magnetic multi-walled carbon nanotubes by response surface methodology, Water Sci. Technol., 76 (2017) 2593–2602.

[27] S. Chattoraj, N.K. Mondal, K. Sen, Removal of carbaryl insecticide from aqueous solution using eggshell powder: a modeling study, Appl. Water Sci., 8 (2018) 1–9.

[28] M. Nikou, A. Samadi-Maybodi, K. Yasrebi, E. Sedighi-Pashaki, Simultaneous monitoring of the adsorption process of two organophosphorus pesticides by employing GO/ZIF-8 composite as an adsorbent, Environ. Technol. Innovation, 23 (2021) 101590, doi: 10.1016/j.eti.2021.101590.

[29] M. Foschi, P. Capasso, M.A. Maggi, F. Ruggieri, G. Fioravanti, Experimental design and response surface methodology applied to graphene oxide reduction for adsorption of triazine herbicides, ACS Omega, 6 (2021) 16943–16954.

[30] C.D. Atemkeng, G.S. Anagho, R.F.T. Tagne, L.A. Amola, A. Bopda, T. Kamgaing, Optimization of 4-nonylphenol adsorption on activated carbons derived from safou seeds using response surface methodology, Carbon Trends, 4 (2021) 100052, doi: 10.1016/j.cartre.2021.100052.

[31] M.H. Dehghani, A.H. Hassani, R.R. Karri, M. Yousefi, Process optimization and enhancement of pesticide adsorption by porous adsorbents by regression analysis and parametric modelling, Sci. Rep., 11 (2021) 1–15.

[32] N.D. Mu'azu, N. Jarrah, T.S. Kazeem, M. Zubair, M. Al-Harthi, Bentonite-layered double hydroxide composite for enhanced aqueous adsorption of Eriochrome Black T, Appl. Clay Sci., 161 (2018) 23–34.

[33] S. Chakraborty, I. Sarkar, K. Haldar, S.K. Pal, S. Chakraborty, Synthesis of Cu-Al layered double hydroxide nanofluid and characterization of its thermal properties, Appl. Clay Sci., 107 (2015) 98–108.

[34] M.H. Tajuddin, N. Yusof, I.W. Azelee, W.N.W. Salleh, A.F. Ismail, J. Jaafar, F. Aziz, K. Nagai, N. Faizah Razali, Development of copper-aluminum layered double hydroxide in thin film nanocomposite nanofiltration membrane for water purification process, Front. Chem., 7 (2019) 3, doi: 10.3389/fchem.2019.00003.

[35] S. Saini, J. Chawla, R. Kumar, I. Kaur, Response surface methodology (RSM) for optimization of cadmium ions adsorption using C16-6-16 incorporated mesoporous MCM-41, SN Appl. Sci., 1 (2019) 1–10.

[36] N. Habib, A. Harat, D.Begin, M. Guerioune, Ni–Zn hydroxide-based bi-phase multiscale porous nanohybrids:

physico-chemical properties, Appl. Nanosci., 10 (2020) 2467–2477.
[37] A.A. Mohammed, A.A. Najim, T.J. Al-Musawi, A.I. Alwared, Adsorptive performance of a mixture of three nonliving algae classes for nickel remediation in synthesized wastewater, J. Environ. Health Sci. Eng., 17 (2019) 529–538.
[38] A. Khatoon, H. Rahman, N. Rahman, Studies on the development of spectrophotometric method for the determination of haloperidol in pharmaceutical preparations, Quim. Nov., 35 (2012) 392–397.
[39] K. El Hassani, B.H. Beakou, D. Kalnina, E. Oukani, A. Anouar, Effect of morphological properties of layered double hydroxides on adsorption of azo dye methyl orange: a comparative study, Appl. Clay Sci., 140 (2017) 124–131.
[40] S.L. Kareem, A.A. Mohammed, Removal of tetracycline from wastewater using circulating fluidized bed, Iraqi J. Chem. Pet. Eng., 21 (2020) 29–37.
[41] K.M. Parida, L. Mohapatra, Carbonate intercalated Zn/Fe layered double hydroxide: a novel photocatalyst for the enhanced photo degradation of azo dyes, Chem. Eng. J., 179 (2012) 131–139.
[42] N.R. Palapa, T. Taher, B.R. Rahayu, R. Mohadi, A. Rachmat, A. Lesbani, CuAl LDH/rice husk biochar composite for enhanced adsorptive removal of cationic dye from aqueous solution, Bull. Chem. React. Eng. Catal., 15 (2020) 525–537.
[43] J. Liu, P. Yao, Z.M. Ni, Y. Li, W. Shi, Jahn–Teller effect of Cu-Mg-Al layered double hydroxides, Wuli Huaxue Xuebao/Acta Phys. - Chim. Sin., 27 (2011) 2088–2094.
[44] H.A. Tabti, M. Adjdir, A. Ammam, B. Mdjahed, B. Guezzen A. Ramdani, Facile synthesis of Cu-LDH with different Cu/Al molar ratios: application as antibacterial inhibitors, Res. Chem. Intermed., 46 (2020) 5377–5390.
[45] Q. Zhang, Q. Jiao, F. Leroux, P. Tang, D. Li, Y. Feng, Antioxidant intercalated hydrocalumite as multifunction nanofiller for poly(propylene): synthesis, thermal stability, light stability, and anti-migration property, Polym. Degrad. Stab., 140 (2017) 9–16.
[46] C. Forano, T. Hibino, F. Leroux, C. Taviot-Guého, Chapter 13.1 Layered Double Hydroxides, in: Developments in Clay Science, 2006, pp. 1021–1095.
[47] L.S. Tabana, R.P. Ledikwa, S.M. Tichapondwa, Adsorption of phenol from wastewater using modified layered double hydroxide clay, Chem. Eng. Trans., 76 (2019) 1267–1272.
[48] S. Nishimura, A. Takagaki, K. Ebitani, Monodisperse iron oxide nanoparticles embedded in Mg-Al hydrotalcite as a highly active, magnetically separable, and recyclable solid base catalyst, Bull. Chem. Soc. Jpn., 83 (2010) 846–851.
[49] M. Bhowmik, K. Deb, A. Debnath, B. Saha, Mixed phase Fe_2O_3/Mn_3O_4 magnetic nanocomposite for enhanced adsorption of methyl orange dye: neural network modeling and response surface methodology optimization, Appl. Organomet. Chem., 32 (2018) 1–17.
[50] J.O. Ighalo, A.A. Adelodun, A.G. Adeniyi, C.A. Igwegbe, Modelling the effect of sorbate-sorbent interphase on the adsorption of pesticides and herbicides by historical data design, Iran. J. Energy Environ., 11 (2020) 4, doi: 10.5829/IJEE.2020.11.04.02.
[51] A.L. Ahmad, S. Ismail, S. Bhatia, Optimization of coagulation–flocculation process for palm oil mill effluent using response surface methodology, Environ. Sci. Technol., 39 (2005) 2828–2834.
[52] M. Darvishmotevalli, A. Zarei, M. Moradnia, M. Noorisepehr, H. Mohammadi, Optimization of saline wastewater treatment using electrochemical oxidation process: prediction by RSM method, MethodsX, 6 (2019) 1101–1113.
[53] M.R. Rezaei Kahkha, M. Kaykhaii, G. Ebrahimzadeh, Optimization of affective parameter on cadmium removal from an aqueous solution by *Citrullus colocynthis* powdered fruits by response surface, Health Scope, 4 (2015) 1, doi: 10.17795/jhealthscope-20667.
[54] R. Singh, R. Bhateria, Optimization and experimental design of the Pb^{2+}adsorption process on a nano-Fe_3O_4-based adsorbent using the response surface methodology, ACS Omega, 5 (2020) 28305–28318.
[55] A.A. Mohammed, S.L. Kareem, Adsorption of tetracycline fom wastewater by using Pistachio shell coated with ZnO nanoparticles: equilibrium, kinetic and isotherm studies, Alexandria Eng. J., 58 (2019) 917–928.
[56] K.K. Hummadi, Optimal operating conditions for adsorption of heavy metals from an aqueous solution by an agriculture waste, Iraqi J. Chem. Pet. Eng., 22 (2021) 27–35.
[57] D. Balarak, Y. Mahdavi, E. Bazrafshan, A.H. Mahvi, Y. Esfandyari, Adsorption of fluoride from aqueous solutions by carbon nanotubes: determination of equilibrium, kinetic, and thermodynamic parameters, Fluoride, 49 (2016) 71–83.
[58] L.F.M. Ali, A.A. Mohammed, Batch heavy metals biosorption by *Punica granatum* peels: equilibrium and kinetic studies, J. Eng., 21 (2015) 161–178.
[59] A.A. Mohammed, F.E. Al-Damluji, T.J. Al-Musawi, Equilibrium and thermodynamic studies of reactive orange dye biosorption by garden grass, J. Eng., 21 (2015) 82–97.
[60] N.D. Mu'azu, M. Zubair, I. Ihsanullah, Process optimization and modeling of phenol adsorption onto sludge-based activated carbon intercalated mgalfe ternary layered double hydroxide composite, Molecules, 26 (2021) 4266, doi: 10.3390/molecules26144266.
[61] F. Ghorbani, S. Kamari, Application of response surface methodology for optimization of methyl orange adsorption by Fe-grafting sugar beet bagasse, Adsorpt. Sci. Technol., 35 (2017) 317–338.
[62] N. Sohrabi, R. Mohammadi, H.R. Ghassemzadeh, S.S. Heris, Design and synthesis of a new magnetic molecularly imprinted polymer nanocomposite for specific adsorption and separation of diazinon insecticides from aqueous media, Microchem. J., 175 (2022) 1–32.
[63] J.I. Soc, B. Diler, K. Dilek, Removal of bentazon and metalaxyl pesticides from aqueous solutions by using chestnut shells: process optimization by experimental design, adsorption kinetics and isotherm analysis, J. Indian Chem. Soc., 96 (2019) 1155–1161.
[64] S. Chattoraj, N.K. Mondal, B. Sadhukhan, P. Roy, T.K. Roy, Optimization of adsorption parameters for removal of carbaryl insecticide using neem bark dust by response surface methodology, Water Conserv. Sci. Eng., 1 (2016) 127–141.
[65] H. Esfandian, A. Samadi-Maybodi, M. Parvini, B. Khoshandam, Development of a novel method for the removal of diazinon pesticide from aqueous solution and modeling by artificial neural networks (ANN), J. Ind. Eng. Chem., 35 (2016) 295–308.